State-to-state dynamics and doubly differential cross sections of the reaction of chlorine atoms with CH_4 ($\nu_3 = 1, J$)

William R. Simpson, Andrew J. Orr-Ewing, and Richard N. Zare

Stanford University,
Department of Chemistry
Stanford, CA 94305

ABSTRACT

A mixture of methane and chlorine molecules in a helium carrier is expanded into a vacuum chamber using a pulsed valve. Polarized laser photolysis of Cl_2 at 355 nm is used to produce chlorine atoms with a sharply peaked speed distribution and a known angular distribution. Methane molecules are excited in the ν_3 mode by infrared absorption on the R(0) fundamental transition, which results in methane in the $\nu_3 = 1$, $J = 1$ state. Following a 100 ns time delay to allow for reaction, HCl ($v' = 1$, J') product molecules are detected by (2+1) resonance enhanced multiphoton ionization (REMPI). The resulting photoions are detected with both mass and velocity resolution using a linear time-of-flight mass spectrometer (TOF-MS). An analysis of the time dependence of the ion signal allows us to determine the differential scattering cross section for the specific rovibrational state ionized. The TOF data show a change in the product angular distribution with J', and thus demonstrate the importance of measuring doubly differential cross sections for elucidating the dynamics of this reaction system.

1. INTRODUCTION

Since the time of Ahrrenius, we have known that the total energy of a reacting system, in the form of a temperature, affects its reaction rate and dynamics. More recently, we have begun the process of separating the effects of reagent vibrational, rotational, and translational energies on reactivity and dynamics. In this and other laboratories,[1-3] experiments have shown that vibrational energy can have a profound influence on chemical reactivity, even for low levels of vibrational excitation.

The use of infrared radiation to excite reagents vibrationally also affords us control of the rotational state of the reagent, and thus provides the opportunity to study the effects of rotational energy. This control of rovibrational energy in the entrance valley of reactions allows us to study the initial-state dependence and to build up a picture of the reagent side of the reaction in much the same way that final-state measurements on the product side can be used to understand the exit valley. In addition, measurement of velocity projections and angular momentum distributions of the products with known velocity distributions for the reagents can give us information about vector correlations involved in the reaction.[4] In this paper we investigate the state-to-state reaction

$$Cl(^2P_{3/2}) + CH_4(\nu_3 = 1, J = 1) \rightarrow HCl(v' = 1, J') + CH_3 \qquad (1)$$

and measure the HCl product angular distribution for different HCl product internal states.

2. BACKGROUND

The reaction of Cl with ground state CH_4 is nearly thermoneutral with an endothermicity of 1.89 ± 0.10 kcal/mol (661 ± 35 cm^{-1}) and a barrier of ca. 3.5 kcal/mol (1220 cm^{-1}) .[5] A quantum mechanical

0-8194-1085-3/93/$4.00

calculation of the transition state energy and structure has been performed by Truong et al.,[6] who predict a linear transition state. Although the past work on this system is sparse, it is energetically and kinematically similar to that of $O(^3P)$ + hydrocarbons studied by Luntz et al.[7] In these reactions, they found that the OH formed from the reaction could be described by a model in which the hydrocarbon radical could be viewed as a structureless particle. The rotational distribution was quite cold, peaking at the lowest level of rotational energy. This finding was interpreted to mean that the transition state is linear, with little torque applied to the HO during its breakup. It was also argued that the transition state would not rotate on the time scale of the reaction, and thus the product should be back scattered with respect to the direction of the initial relative velocity of the oxygen atom.

3. EXPERIMENTAL

The experimental apparatus is shown schematically in figure 1. It consists of a reaction chamber and a differentially pumped detection chamber. Reagents are expanded via a pulsed nozzle into the reaction chamber where they are intersected by the photolysis and infrared pumping laser beams. Products are ionized by the probe laser, and ions are extracted through a slit into the detection chamber where they are detected by a chevron microchannel plate particle multiplier. The reaction chamber is typically operated at pressures of $<3x10^{-5}$ Torr, while the detection chamber is maintained at $<6x10^{-7}$ Torr.

Chlorine atoms are generated by photolysis of Cl_2 at 355 nm (50 mJ in a 1 mm diameter spot) with the ultraviolet radiation made by frequency tripling a Nd:YAG laser (Quantel YG-581-20). Previous

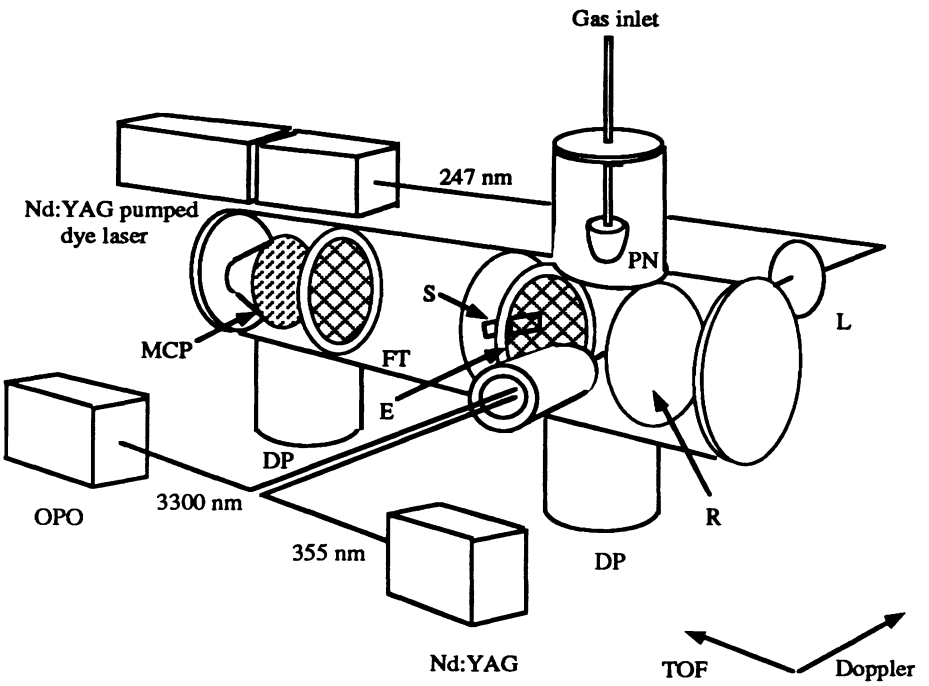

Figure 1: Schematic diagram of the experimental apparatus. The two axes along which velocity resolution is obtained are shown at the bottom right. The abbreviations used are: PN pulsed nozzle, L lens, DP diffusion pump, OPO optical parametric oscillator, MCP microchannel plates, E extractor plate, R repeller plate, S slit, FT flight tube.

studies of this photolysis have shown it to produce almost exclusively ground state atoms (98%) with a perpendicular-type angular distribution with an anisotropy parameter, $\beta = -1$.[7,8] As this photolysis produces primarily ground state atoms, we consider only this reaction channel. The Cl atoms have an energy of 506 meV (4086 cm^{-1}) about the center-of-mass of the Cl_2 that was photolyzed, and 159 meV (1282 cm^{-1}) in the center-of-mass frame of the reaction. Relative motion of the Cl_2 and CH_4 molecules is reduced by coexpanding a mixture of 4% Cl_2, 40% CH_4 and 56% He, total pressure 500 Torr, through a pulsed nozzle. Cooling in the expansion produces an effective translational temperature estimated to be around 15 K. Using this approximate temperature, the spread in collision energies about the center of mass is calculated to be 44 meV FWHM, which is significantly reduced from the 300 K value of 196 meV.[9]

Methane molecules are excited by infrared absorption on the R(0) line of the fundamental of the ν_3 mode (3030 cm^{-1}). The ν_3 mode of CH_4 is nominally an asymmetric stretch, but also has components of motion orthogonal to the direction of the C-H stretch. The infrared radiation is generated from a Nd:YAG (Spectra Physics DCR-1) pumped lithium niobate optical parametric oscillator (OPO), which produces approximately 2 mJ of IR at 3.3 μm, and is fired slightly before the photolysis laser (about 10 ns). This laser is nearly unpolarized, and is operated at half the repetition rate of the photolysis and probe lasers. Thus, alternate shots can be subtracted to find the IR-induced signal. This background signal subtraction has been checked by verifying that no difference is produced when the OPO is blocked.

The OPO and photolysis beams copropagate through the chamber to prepare the reagents and initiate reaction. Following a 100 ns reaction time, the products are probed quantum state specifically by the counterpropagating REMPI laser pulse. Product HCl (v' = 1, J') molecules are probed by (2+1) REMPI on the (0,1) band of the $E^1\Sigma^+ - X^1\Sigma^+$ transition at about 247 nm.[10-13] Tunable 247 nm light is generated by frequency doubling in a β-barium borate (BBO) crystal the output of a Nd:YAG pumped dye laser (Spectra Physics PDL-3 and DCR-2AG) operating on LD489. The probe beam is gently focused with a 500 mm lens into the middle of the region where the molecules were vibrationally excited and photolyzed, which is also the middle of the extraction region of a linear TOF mass spectrometer. The mass spectrometer signal depends on the mass of the ion formed and the initial velocity of the ion.[14-17] Thus, a measurement of the TOF peak shape is equivalent to a one-dimensional projection of the velocities of the ionized molecules along the axis of the TOF tube. Additionally, the ionization laser has a bandwidth that is smaller than the Doppler width of the product molecules, so only the molecules with a proper Doppler shift to be resonant with the laser are ionized. This Doppler resolution along the probe beam axis provides a second dimension for velocity projection along an orthogonal axis. Thus TOF peaks taken as a function of Doppler shift provide a two-dimensional projection of the velocity of the molecules ionized. We refer to this technique as time-resolved ion pulse spectroscopy (TRIPS). The TRIPS method allows the recording of doubly differential cross sections for this reaction because it is a simple matter to relate the ion signal to the flux of quantum-state resolved product into a solid angle element.

Reagent TOF profiles of the ^{35}Cl mass peak are taken on a fast digital sampling oscilloscope (Tektronix TDS 620) by averaging 160 laser shots in 1.5 ns time bins. At different Doppler detunings, 19 TOF profiles are obtained by slowly scanning the probe laser over the transition while recording 160-shot-averaged TOF profiles. This results in a two dimensional image of the reagent velocity distribution. Reactive TOF profiles of the $H^{35}Cl$ mass peak are taken by averaging 40 laser shots (in 1 ns bins) with the OPO firing and subtracting an average of 40 laser shots taken with the OPO blocked. This subtraction procedure is repeated many times until the signal-to-noise ratio is acceptable. Typical reactive TOF spectra are the result of 1000 to 4000 laser shots with the OPO on and an equal number of shots with the IR laser off. Between 5 and 50 ions with m/z = 36 are formed per laser shot, which is a low enough level to be free from space charge distortions. It has also been found that the ion signals are independent of total ion yield,

which provides additional evidence that space charge distortion is not a problem. Checks for systematic errors in the subtraction procedure were performed by separately blocking the OPO and photolysis lasers. Blocking the OPO resulted in no difference signal, and blocking the photolysis laser beam results in a signal from the energy transfer background described in section 4.2.

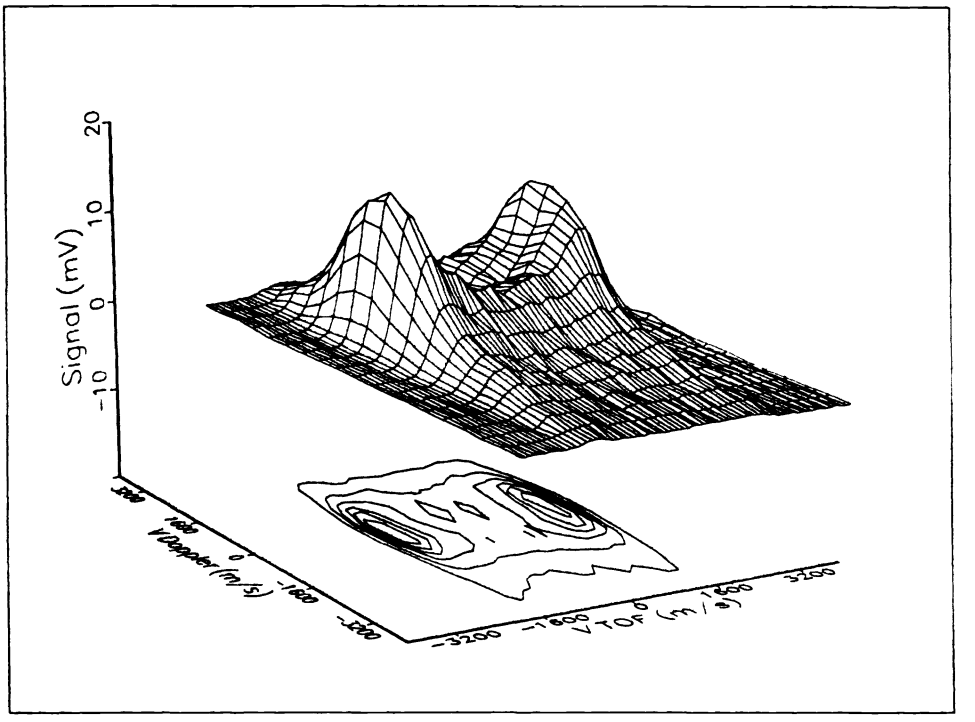

Figure 2: Two dimensional velocity projection of chlorine atoms, with velocity resolution along the time-of-flight and laser propagation axes.

4. DATA AND ANALYSIS

4.1. Cl_2 photodisociation

Two-dimensional velocity profiles of the Cl atoms resulting from the photodissociation of Cl_2 at 355 nm were taken for three reasons: (1) The energy and anisotropy parameters are known for Cl_2 at 355 nm, so this signal provides a calibration and check on the instrument. (2) The experimental instrument function can be determined by simulation of the data for this photolysis. This function will be necessary to simulate experimental TOF data. (3) Measurements of the velocity projection as a function of photolysis - probe delay show that negligible flyout occurs on the 100 ns time scale used for the reactive experiments.

Cl atoms are probed by (2+1) REMPI on the $^4P^0_{3/2} - {}^2P^0_{3/2}$ transition at 240.53 nm.[18] Figure 2 shows the two-dimensional velocity projection of Cl atoms formed by photolysis, with the polarization of the photolysis and probe lasers pointing out of the plane of the image. If the blurring along the Doppler and TOF axes were equivalent, the image would be a circle, but the Doppler resolution is much worse than the TOF resolution, so the image is washed out along the Doppler dimension. The double-peaked, symmetric form along the TOF axis is a consequence of the anisotropy of the Cl_2 photodissociation: Cl atoms are formed with velocities preferentially perpendicular to the electric vector of the linearly polarized

photolysis laser (E_{phot}), and this velocity distribution is retained immediately after laser ionization. Those Cl^+ ions with initial velocities antiparallel to the TOF axis are turned around by the repeller plate voltage and reach the detector at a later time than those ions with velocities parallel to this axis. The TOF profile therefore corresponds to a projection of the Cl velocity distribution, which is cylindrically symmetric about E_{phot}, onto the TOF axis, and the peaks in the wings arise because of 'edge-brightening'. Anticipating the data presented in section 4.3, we note that the form of the Cl-atom TOF profile is largely retained in the HCl product of the reaction of Cl with CH_4, regardless of the nature of the differential scattering cross section. Although the Doppler resolution is poor in figure 2, the power-broadened laser linewidth is comparable to the Doppler width of the Cl photofragments (and HCl reaction products). Compared to a broadband linewidth, this Doppler selectivity makes a marked improvement in the resolution of the TOF profile when the ionization laser frequency is set at the Doppler line center. This improvement arises because we then obtain TOF profiles that are a composite of profiles for different Doppler shifts within our laser bandwidth, and the TOF profile widths in this region are nearly independent of the Doppler shift. When we analyze the TOF profiles of reactive signals, only the profile at Doppler center is taken, because it contains the most information and has the strongest signal.

4.2. Integral cross sections

The integral cross sections for formation of HCl in v' = 1 were measured by charge integrating the ion signal over a mass gate set on the H^+ fragment mass from the REMPI of HCl. This fragment mass provides a signal proportional to the number of HCl molecules in the quantum state being ionized.[10,12,18,19] Pulsed nozzle backing pressures were varied from 250 Torr to 700 Torr, and reaction time delays were varied from 50 ns to 400 ns to check for clustering, flyout, and collisional relaxation. Over these ranges, no change in the quantum state distribution was found. A background signal from HCl contaminant in v = 0, ionized on the V - X (6,0) transition (see Rohlfing et al.[20]), was removed by using the alternate shot IR subtraction procedure described in the experimental section, since that signal does not depend on infrared excitation of the methane molecules. This contamination of HCl also leads to HCl(v = 1) molecules via a pathway involving near resonant energy transfer from CH_4 ($\nu_3 = 1$). This background was assigned to this pathway because it depends on the OPO but not on the photolysis laser. Additionally, the background increases approximately linearly with pump-probe time delay and increases when HCl is added to the reaction mix. Its TOF peak is narrow, being approximately Gaussian with FWHM of 7.5 ns, which is less than 1 ns wider than the instrument resolution function. Thus the HCl product has little kinetic energy, which provides additional evidence for this assignment. The quantum state distribution of this background was measured and subtracted from the total reactive signals to recover the integral reactive cross section. This correction was typically less than 5 percent. Figure 3 shows the integrated ion signal as a function of rotational quantum number. The error bars shown are two standard deviations, and represent statistical errors from six independent distributions taken over a range of conditions. The figure presents integral ion signals, not population distributions, because deviations from the correction factors of Rohlfing et al.[20] were found under our experimental conditions. Work is in progress to calibrate this transition. Since the correction factors are probably slowly varying with J', this distribution should be representative of the general form of the population distribution.

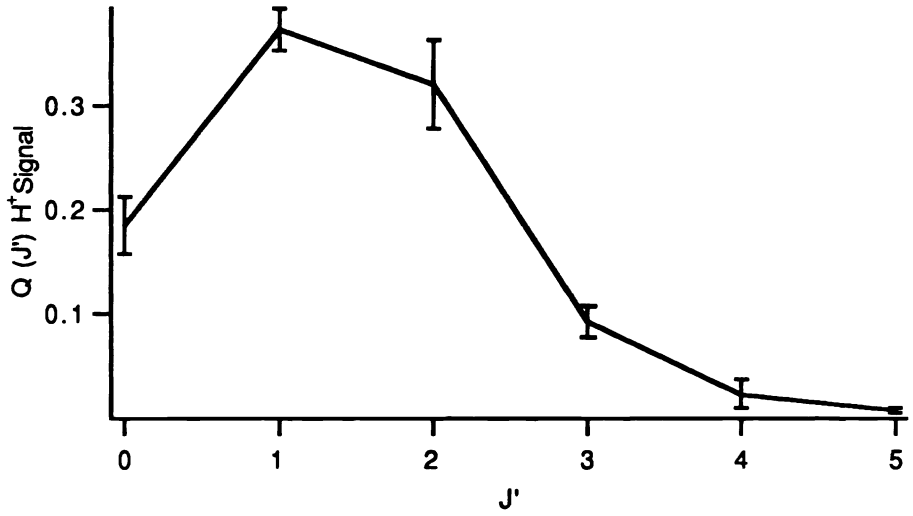

Figure 3: Integrated ion signal at m/z = 1 for each rotational quantum state of the HCl(v' = 1, J') reaction product. The error bars represent two standard deviations calculated from six data sets. A calibration of the REMPI signal is required to convert to relative populations.

4.3. Differential cross sections

Differential cross sections for this reaction were extracted from reactive TOF profiles measured at Doppler line center using the following procedure. It was first assumed that the CH_3 product of the reaction does not contain any internal energy, or that it is small in comparison to the experimental uncertainties. We will see later that this approximation is supported by the experimental data. Within this assumption, we know the final translational energy by energy balance, and thus we know that the HCl product will be distributed on a sphere about the center of mass of the collision system with a radius defined by this energy balance. Figure 4 shows the lab frame velocity distribution of the Cl atoms along with a scattering diagram for one particular reactive collision. In order to know the lab frame velocity distribution, we add vectorially the center-of-mass velocity (v_{CM}) for a collision to the center-of-mass scattering velocity (v_{CM}^{HCl}), and the speed $|v_{LAB}^{HCl}|$ is simply given by trigonometry:

$$\left|v_{LAB}^{HCl}\right| = \sqrt{\left|v_{CM}^{HCl}\right|^2 + \left|v_{CM}\right|^2 + 2\left|v_{CM}^{HCl}\right|\left|v_{CM}\right|\cos\theta} \qquad (2a)$$

$$\left|v_{LAB}^{HCl}\right| \approx \left|v_{CM}\right| + \left|v_{CM}^{HCl}\right|\cos\theta \qquad (2b)$$

In the limit that the recoil velocity is small compared to the center-of-mass velocity in the lab frame, the second approximate equation may be substituted. In our case, the recoil velocity of the HCl in the center-of-mass is about 370 m/s and the center-of-mass velocity is about 1150 m/s in the lab frame, so we use the approximation from equation (2b). The reaction changes the direction of the HCl by an angle γ from the inital Cl direction. Thus the anisotropy of the HCl product will be given by [21]

$$\beta = P_2(\cos\gamma)\beta_{Photolysis} \approx \beta_{Photolysis} \qquad (3)$$

where the approximation is valid for small angles γ. Since our maximum angle of γ is 18 degrees, we use the approximate form of equation (3).

For any particular scattering projection, cosθ, we use the speed and anisotropy from equations (2) and (3) to generate a three-dimensional velocity distribution $I(v_x,v_y,v_z;|v_{CM}^{HCl}|,\cos\theta)$. This distribution is projected into the plane containing the TOF and probe laser axes, and is then integrated over the probe laser direction with a Doppler resolution function $D(v_x)$ to give a one-dimensional velocity distribution

$$I(v_Z;\left|v_{CM}^{HCl}\right|,\cos\theta) = \int dv_Y \int dv_X D(v_X) I(v_X,v_Y,v_Z;\left|v_{CM}^{HCl}\right|,\cos\theta) \qquad (4)$$

This function is then blurred with the instrumental TOF resolution function T(v) to give an experimental signal for that scattering projection $S(v;|v_{CM}^{HCl}|,\cos\theta)$

$$S(v;\left|v_{CM}^{HCl}\right|,\cos\theta) = \int dv_Z T(v-v_Z) I(v_z;\left|v_{CM}^{HCl}\right|,\cos\theta) \qquad (5)$$

The forms of these functions will be similar to the double-peaked TOF profiles arising from Cl_2 photolysis because of the near conservation of the photolysis anisotropy in the reaction products shown in equation (3). We might expect that the TOF profiles would also be sensitive to rotational alignment of the reaction

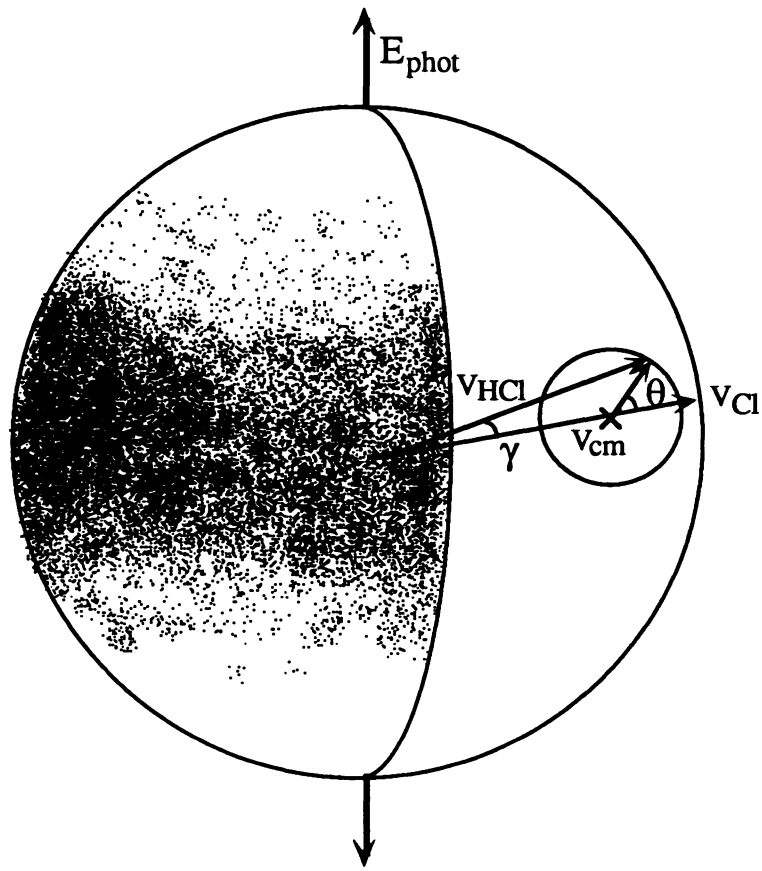

Figure 4: The kinematics and anisotropy of the reaction: Cl atoms from the 355 nm photolysis of Cl_2 expand outwards on the surface of a sphere. The shading indicates the probability distribution for $\beta = -1$. Inset is a Newton diagram for the reaction of Cl with CH_4. For the experimental conditions described in section 3, the velocity of the center of mass and the relative velocity lie parallel to the Cl atom velocity. HCl(v' = 1, J') is scattered on the surface of the small sphere, with a radius determined by energy conservation.

products and other vector correlations.[15] However, profiles recorded with horizontal and vertical linear polarizations of the probe laser were observed to have the same form. This is probably a consequence of probing on the Q branch of a two-photon Σ - Σ transition, which is insensitive to rotational alignment; if desired, we can look for the presence of aligned products via alternative spectroscopic transitions. The measured experimental signal S(v) will be given by the integral of the product of the differential cross section $\sigma(\cos\theta)$ and the signal functions $S(v;|v_{CM}^{HCl}|,\cos\theta)$

$$S(v) = \int d(\cos\theta)\sigma(\cos\theta)S(v;|v_{CM}^{HCl}|,\cos\theta) \tag{6}$$

To limit the number of parameters used for fitting, we expand the differential cross section in a Legendre basis

$$\sigma(\cos\theta) = \sum_{l=0}^{\infty} c_l P_l(\cos\theta) \tag{7}$$

and substitute into the equation for the S(v)

$$S(v) = \int d(\cos\theta)\sum_{l=0}^{\infty} c_l P_l(\cos\theta)S(v;|v_{CM}^{HCl}|,\cos\theta) \tag{8a}$$

$$S(v) = \sum_{l=0}^{\infty} c_l S_l\left(v;|v_{CM}^{HCl}|\right) \tag{8b}$$

$$S_l\left(v;|v_{CM}^{HCl}|\right) = \int d(\cos\theta)P_l(\cos\theta)S(v;|v_{CM}^{HCl}|,\cos\theta) \tag{8c}$$

Thus, we can recover the Legendre moments of the differential cross section by fitting the data to a linear combination of the $S_l(v;|v_{CM}^{HCl}|)$ functions. To evaluate the integral involved in the equation for $S_l(v;|v_{CM}^{HCl}|)$, it is transformed into a summation

$$S_l\left(v;|v_{CM}^{HCl}|\right) \approx \sum_{i=-N}^{N} \frac{1}{2N+1} P_l\left(\frac{i}{N+1/2}\right) S\left(v;|v_{CM}^{HCl}|,\frac{i}{N+1/2}\right) \tag{9}$$

This formula is used with N = 5 to generate the Legendre signal functions for P_0 to P_3. The laser propagation resolution function is a Lorentzian of FWHM equal to the HCl Doppler width, and the TOF resolution functon is an 8 ns FWHM Gaussian. The TOF data are fitted to a linear combination of these functions S_0 to S_3 along with a 7.5 ns FWHM Gaussian centered at zero velocity which describes the energy transfer signal. The fit coefficients are then used to regenerate the differential scattering cross section by substitution into equation (7). Figure 5 and figure 6 show the fit and the results of this fitting procedure for two values of J' of the HCl (v' = 1).

5. DISCUSSION

Traditional experiments for measuring differential scattering cross sections typically make use of crossed molecular beams, and gave rise to the notions of stripping, rebound and complex-mode reaction mechanisms.[22] Such experiments were not, however, generally sensitive to the scattering dynamics on a quantum state resolved level. Recently several experimental methods have been developed to measure doubly differential cross sections, by making use of techniques such as ion imaging,[23] one and two-dimensional Doppler spectroscopy,[24] and Rydberg atom TOF translational spectroscopy.[25] In this study we have taken the process a step further by resolving doubly differential cross sections for state selected reagents. The analysis of the data presented in the preceding section provides substantial detail of the dynamics of reaction (1) which would not come from separate measurements of rovibrational state populations and quantum state averaged differential scattering cross sections.

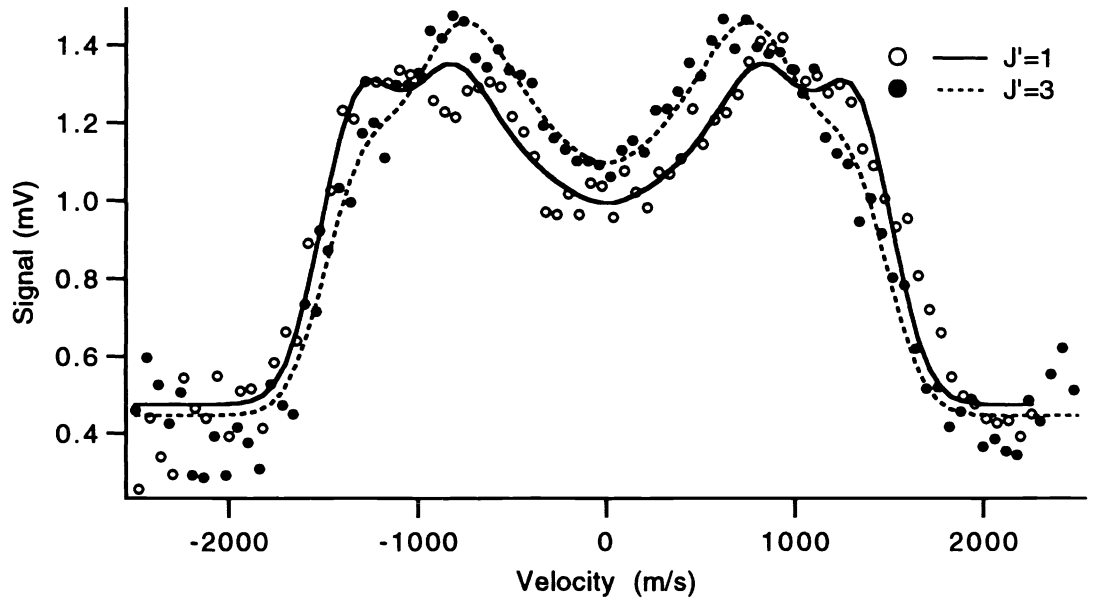

Figure 5: TOF profiles for HCl(v' = 1, J' = 1) and HCl(v' = 1, J' = 3) together with fits to the data (lines) performed as described in the text. For clarity, the central component of the profiles, attributed to energy transfer between CH_4 and HCl, has been subtracted out.

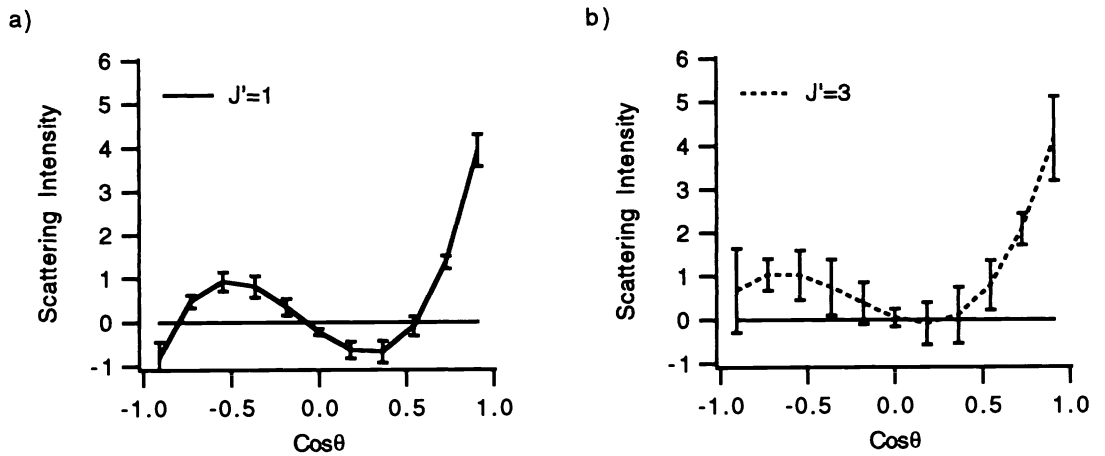

Figure 6: Extracted differential cross sections for (a) J' = 1 and (b) J' = 3. The data presented here are the averages of at least three fits to TOF profiles, with estimated errors shown.

Even without the fitting procedure described in section 4.3, the TOF data demonstrate some interesting effects. Examining the J' = 1 peak, we find significant signal occurs beyond the velocity of the center-of-mass. This signal implies at least some of the products of the reaction producing HCl(v' = 1, J' = 1) are forward scattered. The fit for this product state shows the extent of forward scattering. However, it does go slightly negative in some regions, and we believe this unphysical result is an artifact of an overcompensation by the higher order Legendre terms in our truncated expansion. The observed forward scattering behavior is noteworthy because the signal from product that has significant energy in the

CH_3 internal modes would appear near the center-of-mass speed, thus at $\cos\theta = 0$ in this analysis. We reach this conclusion because insufficient energy is available to the reaction products to populate CH_3 vibrational modes and still account for the width of the TOF profile. The energy available to internal CH_3 excitation, HCl rotation and product translation is about 750 cm^{-1}, and hence $v = 1$ of the umbrella mode of CH_3, with a frequency of 606 cm^{-1}, is just energetically accessible, but if populated, leaves at most 144 cm^{-1} for CH_3 and HCl translation. The experimental data therefore imply that for production of HCl($v' = 1$), the remaining energy from the reaction is preferentially channelled into product translation as opposed to CH_3 internal mode excitation.

The HCl($v' = 1, J' = 3$) product TOF profile is significantly different from the lower J' product shown. This result clearly demonstrates that the scattering dynamics are a function of J' in this system. Taking integrated areas for $\cos\theta > 0$ and $\cos\theta < 0$ as a measure of forward versus backward scattering, the analysis shows a differential scattering cross section for the $J' = 3$ product that has a larger back scattering component than the $J' = 1$ product does, along with a smaller strongly forward scattered peak. By analogy with $O(^3P)$ + hydrocarbons, we would expect the cold rotational distribution to indicate back scattering. We would also expect that higher J' products would be formed with more forward peaked differential scattering cross sections. In the experiment, neither of these is seen, and we tentatively assign this behavior to the fact that we have prepared a particular vibrational mode of CH_4 in these experiments. If the form of the ν_3 mode of the CH_4 is not significantly perturbed by collinear approach of the Cl atom, then the component of ν_3 that corresponds to C-H motion that is not parallel to the equilibrium CH bond direction can couple to rotation of the HCl product, thus giving rotational excitation in back-scattered products. This behavior is mode specific, and would not be expected, for example, in the reaction of Cl with CH_4 excited in the ν_1 symmetric stretch.

The origin of the rotationally cold, forward-scattered HCl is surprising, because a simple, impulsive model of the rotational excitation of the products predicts that the Cl-H-CH_3 bond angle in the transition state must take values $\leq 5^o$ for the HCl to be formed in rotational states $J' \leq 2$.[26] We must therefore postulate either that the transition-state bond angle is constrained to values $\leq 5^o$, which seems to be at odds with the differential scattering cross section data, or that the dynamics is not occurring in the impulsive, sudden limit: the release of energy along the C-H coordinate might be sufficiently gradual, as the Cl atom strips the H atom, that HCl rotation is not induced. This latter model could relate to the fact that we are studying a vibrationally adiabatic channel in this reaction. Simple calculations, based on the minimum barrier height for the vibrationally adiabatic reaction being the reaction endothermicity, predict that the Cl atom has a speed of the order of five times faster than the tangential velocity of an H atom in CH_4 rotating in $J = 1$. However, the vibrationally adiabatic PES for $v = 1$ to $v' = 1$ reaction should show a well in the region of hydrogen atom transfer because the vibrational frequency of the hydrogen decreases to a minimum at the time of transfer.[27] Classically, this corresponds to chattering of the hydrogen between the methyl radical and chlorine atom. If this chattering motion does occur, then the transition state may be able to rotate on the time scale of the reaction, leading to forward-scattered product while maintaining a near linear Cl-H-CH_3 configuration, and thus inducing little product rotational excitation. This rotation of the transition state is envisaged as corresponding to the CH_4 being turned by the forward motion of the Cl, and is not equivalent to the formation of a complex that survives for several rotational periods.

6. CONCLUSION

We have demonstrated a new technique, time-resolved ion pulse spectroscopy, to examine the scattering properties of products of state-to-state chemical reactions. To our knowledge, the present study represents the first simultaneous determination of scattering and quantum state properties for a truly state-

to-state chemical reaction. TRIPS clearly provides a more detailed look at the reaction of Cl with CH_4 than is possible by measuring separately both the product state integrated scattering distribution and the scattering integrated product state distribution. We have shown that the scattering is a function of J' for this system, and we have also found that a cold product rotational distribution is not necessarily correlated with back scattering.

7. ACKNOWLEDGMENTS

WRS would like to thank the National Science Foundation for a predoctoral fellowship. This work has been supported by the National Science Foundation under grant number CHE 89-21198.

8. REFERENCES

1. F. F. Crim, "Selective excitation studies of unimolecular reaction dynamics," *Ann. Rev. Phys. Chem.*, Vol. 35, pp. 657-691, 1984.
2. A. Sinha, M. C. Hsiao, and F. F. Crim, "Controlling bimolecular reactions: Mode and bond selected reation of water with hydrogen atoms," *J. Chem. Phys.*, Vol. 94, pp. 4928-4935, 1991.
3. M. J. Bronikoswki, W. R. Simpson, B. Gerard, and R. N. Zare, "Bond-specific chemistry: OD:OH product ratios for the reactions H+HOD(100) and H+HOD(001)," *J. Chem. Phys.*, Vol. 95, pp. 8647-8648, 1991.
4. J. P. Simons, "Dynamical Stereochemistry and the Polarization of Reaction Products," *J. Phys. Chem.*, Vol. 91, pp. 5378-5387, 1987.
5. A. R. Ravishankara and P. H. Wine, "A laser flash photolysis-resonance fluorescence kinetics study of the reaction $Cl(^2P) + CH_4 \rightarrow CH_3 + HCl$," *J. Chem. Phys.*, Vol. 72, pp. 25-30, 1980.
6. T. N. Truong, D. G. Truhlar, K. K. Baldridge, M. S. Gordon, and R. Steckler, "Transition state structure, barrier height, and vibrational frequencies for the reaction $Cl + CH_4 \rightarrow HCl + CH_3$," *J. Chem. Phys.*, Vol. 90, pp. 7137-7142, 1989.
7. G. E. Busch, R. T. Mahoney, R. I. Morse, and K. R. Wilson, "Translational spectroscopy: Cl_2 photodissociation," *J. Chem. Phys.*, Vol. 51, pp. 449-450, 1969.
8. Y. Matsumi, K. Tonokura, and M. Kawasaki, "Fine-structure branching ratios and Doppler profiles from photodissociation of the chlorine molecule near and in the ultraviolet region," *J. Chem. Phys.*, Vol. 97, pp. 1065-1071, 1992.
9. W. J. van der Zande, R. Zhang, R. N. Zare, K. G. McKendrick, and J. J. Valentini, "Superthermal widths of the collision energy distributions in hot atom reactions," *J. Phys. Chem.*, Vol. 95, pp. 8205-8207, 1991.
10. T. A. Spiglanin, D. W. Chandler, and D. H. Parker, "Mass-resolved laser ionization spectroscopy of HCl," *Chem. Phys. Lett.*, Vol. 137, pp. 414-420, 1987.
11. D. S. Green, G. A. Bickel, and S. C. Wallace, "(2+1)resonance enhanced multiphoton ionization of hydrogen chloride in a pulsed supersonic jet: spectroscopic survey," *J. Mol. Spec.*, Vol. 150, pp. 303-353, 1991.
12. D. S. Green, G. A. Bickel, and S. C. Wallace, "Resonance enhanced multiphoton ionization of hydrogen chloride in a pulsed supersonic jet: spectroscopy and Rydberg-valence interactions of the $^1\Sigma^+(0^+)$ and $^3\Sigma^-(1,0^+)$ states," *J. Mol. Spec.*, Vol. 150, pp. 354-387, 1991.
13. D. S. Green, G. A. Bickel, and S. C. Wallace, "(2+1) resonance enhanced multiphoton ionization of hydrogen chloride in a pulsed supersonic jet: vacuum wavenumbers of rotational lines with detailed band analysis for excited states of $H^{35}Cl$," *J. Mol. Spec.*, Vol. 150, pp. 388-469, 1991.

14. J. F. Black and I. Powis, "Photofragment investigations of the 280 nm photodissociation of methyl iodide using REMPI I atom detection," *Chem. Phys.*, Vol. 125, pp. 375-388, 1988.
15. M. Mons and I. Dimicoli, "Angular correlation between photofragment velocity and angular momentum measured by resonance enhanced multiphoton ionization detection," *J. Chem. Phys.*, Vol. 80, pp. 4037-4047, 1989.
16. H. J. Hwang and M. A. El-Sayed, "Determination of kinetic energy release for direct photodissociation process by one-dimensional TOF photofragment translational spectroscopy," *Chem. Phys. Lett.*, Vol. 170, pp. 161-166, 1990.
17. L. D. Waits, R. J. Horowitz, and J. A. Guest, "Translational energy study of CH_3 photofragments following $^1(n,\pi^*)$ excitation of acetone," *Chem. Phys.*, Vol. 155, pp. 149-156, 1991.
18. S. Arepalli, N. Presser, D. Robie, and R. J. Gordon, "Detection of Cl atoms and HCl molecules by Resonantly Enhanced Multiphoton Ionization," *Chem. Phys. Lett.*, Vol. 118, pp. 88-92, 1985.
19. D. S. Green and S. C. Wallace, "Two-photon spectroscopy, Rydberg-valence interactions, and superexcited state dissociation of HCl probed by resonance enhanced multiphoton ionization," *J. Chem. Phys.*, Vol. 96, pp. 5857-5877, 1992.
20. E. A. Rohlfing, D. W. Chandler, and D. H. Parker, "Direct measurement of rotational energy transfer rate constants for $H^{35}Cl(v=1)$," *J. Chem. Phys.*, Vol. 87, pp. 5229-5237, 1987.
21. R. Bersohn and S. H. Lin, "Orientation of targets by beam excitation," *Adv. Chem. Phys.*, Vol. 16, pp. 67-100, 1969.
22. R. D. Levine and R. B. Bernstein, "*Molecular reaction dynamics and chemical reactivity*, " Oxford University Press, New York, 1987.
23. T. N. Kitsopoulos, M. A. Buntine, D. P. Baldwin, R. N. Zare, and D. W. Chandler, "Reaction product imaging: The H + D_2 reaction," *Science*, submitted.
24. N. E. Shafer and R. Bersohn, "Two and three dimensional laser induced fluorescence: Application to photodissociation of LiI," *J. Chem. Phys.*, Vol. pp. 4817-4820, 1991.
25. L. Schnieder, K. Seekamp-Rahn, F. Liedeker, H. Steuwe, and K. H. Welge, "Hydrogen exchange reaction H + D_2 in crossed beams," *Faraday Disc. Chem. Soc.*, Vol. 91, pp. 259-269, 1991.
26. H. B. Levene and J. J. Valentini, "The effect of parent internal motion on photofragment rotational distributions: Vector correlation of angular momenta and C_{2v} symmetry breaking in dissociation of AB_2 molecules," *J. Chem. Phys.*, Vol. 87, pp. 2594-2610, 1987.
27. I. W. M. Smith, "Vibrational adiabaticity in chemical reactions," *Acc. Chem. Res.*, Vol. 23, pp. 101-107, 1990.